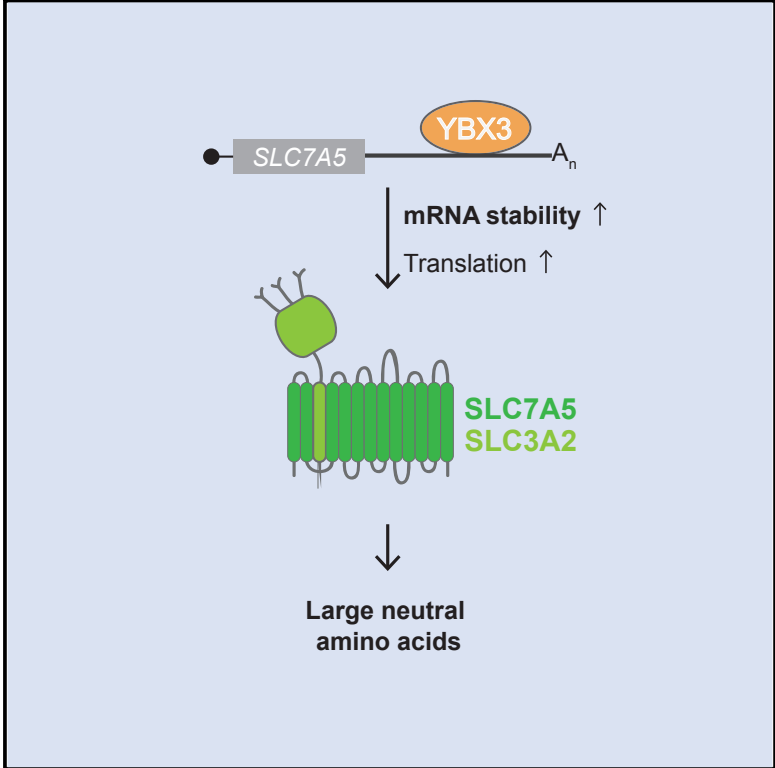# Cell Reports

The RNA-Binding Protein YBX3 Controls Amino Acid Levels by Regulating *SLC* mRNA Abundance

Graphical Abstract

Authors

Amy Cooke, Thomas Schwarzl,
Ina Huppertz, ..., Wolfgang Huber,
Jeroen Krijgsveld, Matthias W. Hentze

Correspondence

huppertz@embl.de (I.H.),
hentze@embl.de (M.W.H.)

In Brief

Cooke et al. uncover an unanticipated function of YBX3 in controlling amino acid levels using a multi-omics approach. The authors demonstrate that YBX3 directly regulates *SLC7A5* mRNA stability. Depletion of YBX3 selectively reduces intracellular levels of SLC7A5-imported amino acids, thus establishing YBX3 as a key regulator of amino acid homeostasis.

Highlights

- Integration of multiple omics datasets reveals genes directly regulated by YBX3

- YBX3 binds and regulates distinct sets of RNAs

- YBX3 binds within the 3′ UTR of *SLC7A5* to stabilize the transcript for translation

- YBX3 emerges as a regulator of large neutral amino acid homeostasis

CellPress

Report

The RNA-Binding Protein YBX3 Controls Amino Acid Levels by Regulating *SLC* mRNA Abundance

Amy Cooke,[1,3] Thomas Schwarzl,[1,5] Ina Huppertz,[1,5,*] Gertjan Kramer,[2,4] Panagiotis Mantas,[1] Anne-Marie Alleaume,[1] Wolfgang Huber,[1] Jeroen Krijgsveld,[1,2] and Matthias W. Hentze[1,6,*]

[1]European Molecular Biology Laboratory (EMBL), Meyerhofstrasse 1, Heidelberg, Germany
[2]German Cancer Research Center (DKFZ), Im Neuenheimer Feld 581, Heidelberg, Germany
[3]Present address: Department of Biochemistry, University of Wisconsin-Madison, Madison, WI 53706, USA
[4]Present address: Laboratory for Mass Spectrometry of Biomolecules, Swammerdam Institute for Life Sciences, University of Amsterdam, Science Park 904, Amsterdam, the Netherlands
[5]These authors contributed equally
[6]Lead Contact
*Correspondence: huppertz@embl.de (I.H.), hentze@embl.de (M.W.H.)
https://doi.org/10.1016/j.celrep.2019.05.039

SUMMARY

Sufficient amino acid supplies are critical for protein synthesis and, thus, cell growth and proliferation. Specialized transporters mediate amino acid exchange across membranes and their regulation is critical for amino acid homeostasis. Here, we report that the DNA- and RNA-binding protein YBX3 regulates the expression of amino acid transporters. To investigate the functions of YBX3, we integrated proteomic and transcriptomic data from cells depleted of YBX3 with analyses of YBX3 RNA binding sites to identify RNAs directly regulated by YBX3. The data implicate YBX3 as a RNA-binding protein that regulates distinct sets of mRNAs by discrete mechanisms, including mRNA abundance. Among direct YBX3 targets, two solute carrier (SLC) amino acid transporters (SLC7A5 and SLC3A2) were identified. We show that YBX3 stabilizes these *SLC* mRNAs and that YBX3 depletion diminishes the expression of SLC7A5/SLC3A2, which specifically reduces SLC7A5/SLC3A2 amino acid substrates. Thus, YBX3 emerges as a key regulator of amino acid levels.

INTRODUCTION

Cold shock proteins are among the most highly conserved protein families from bacteria to humans. This super family is characterized by the presence of one or more cold shock domains (CSDs), enabling these proteins to bind to single-stranded nucleic acids. DNA- and RNA-binding capabilities allow members of this family to perform diverse functions, including regulation of transcription, splicing, translation, and mRNA stability (Kleene, 2018; Lindquist and Mertens, 2018).

The Y-box (YBX) protein family comprises the major group of CSD proteins in humans, which contains three genes, namely, YBX1, YBX2, and YBX3. YBX proteins differ from other CSD proteins in their domain organization, which consists of a central CSD

and unstructured N- and C-terminal regions. However, like other CSD proteins, YBX proteins have been linked to diverse forms of RNA metabolism and many processes, including cell proliferation, DNA repair, multiple stress responses, development, and neurodegenerative and inflammatory diseases (Kleene, 2018; Lindquist and Mertens, 2018; Lyabin et al., 2014; Prabhu et al., 2015).

YBX proteins are highly expressed and bind a broad range of RNAs, creating a challenge to distinguish binding from direct regulation of YBX target RNAs (Kleene, 2018; Lyabin et al., 2014). In addition, YBX proteins have overlapping functions exemplified by phenotypes appearing only if two family members are depleted. For example, the YBX3 knockout mouse develops normally with only minor problems in spermatogenesis and with marginally reduced fertility (Lu et al., 2006). However, a mouse that is hemizygous for both YBX2 and YBX3 (YBX2$^{+/-}$;YBX3$^{+/-}$) is infertile, whereas a double knockout of YBX1/YBX3 is embryonic lethal (Lu et al., 2006; Snyder et al., 2015). The functional redundancy, multilevel regulation, and broad binding by YBX proteins make it difficult to delineate their RNA targets and functional roles.

YBX3 itself has been reported to control gene expression at multiple levels. It was first reported as a DNA-binding factor that regulates the transcription of promoters containing a YBX sequence (Coles et al., 1996; Kudo et al., 1995; Matsumoto and Wolffe, 1998; Sakura et al., 1988; Wolffe and Meric, 1996). Later reports established YBX3 as an RNA-binding protein (RBP) that post-transcriptionally controls translation and mRNA stability (Coles et al., 2004; Davies et al., 2000; Giorgini et al., 2001; Nie et al., 2012). Like other members of the YBX family, YBX3 plays diverse roles in biology, including during development, in spermatogenesis, and cellular differentiation and proliferation (Balda et al., 2003; Giorgini et al., 2002; Lima et al., 2010; Lu et al., 2006; Snyder et al., 2015). However, its functionally relevant RNA-binding targets remain elusive.

To elucidate how YBX3 controls gene expression, we took a multi-omics approach. We first obtained and integrated proteomic and transcriptomic data to assess changes occurring at both the mRNA and translational level upon YBX3 depletion. These data were further integrated with enhanced crosslinking and immunoprecipitation (eCLIP) data for YBX3-RNA complexes to reveal candidates for direct regulation by YBX3. The combined
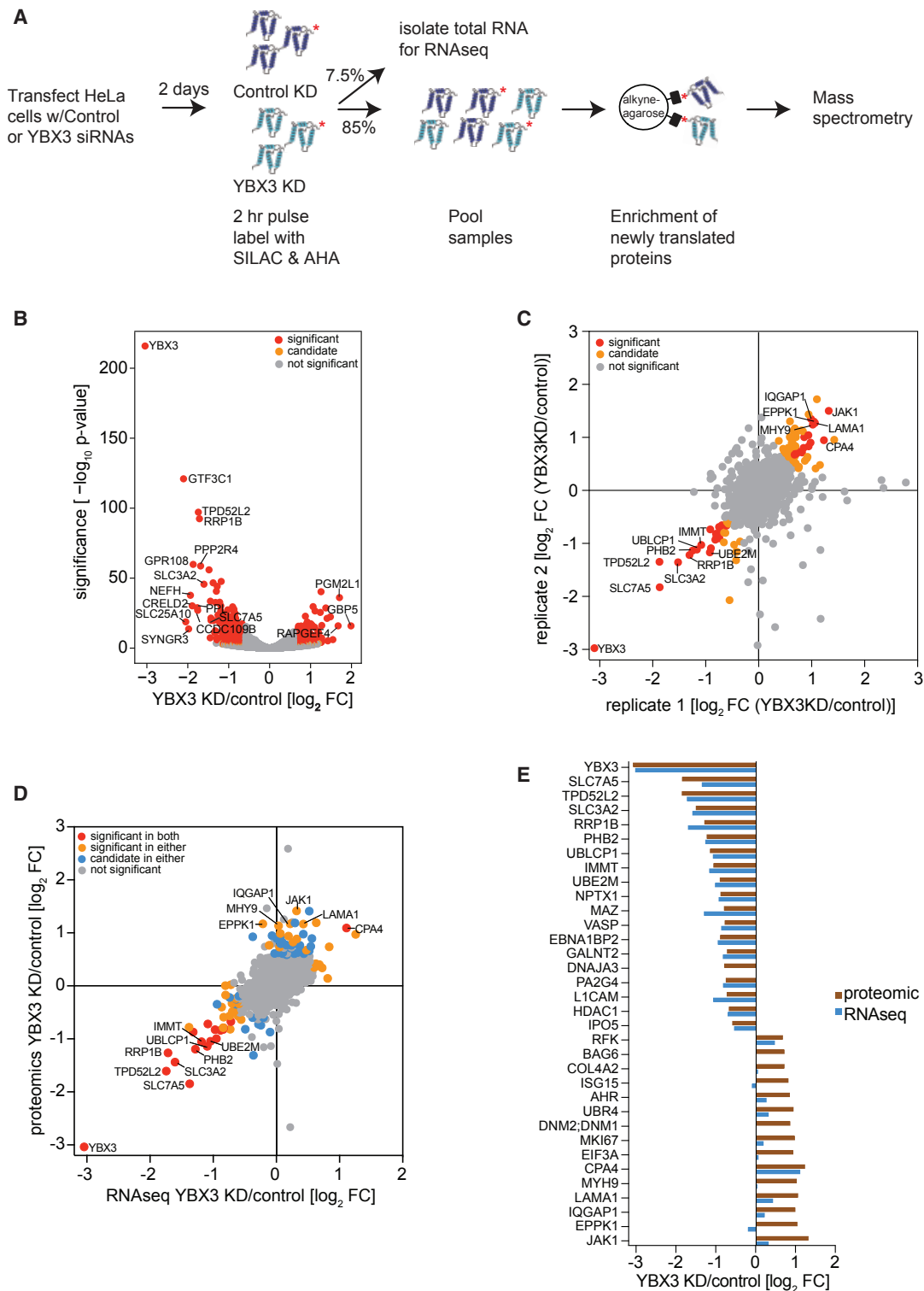
Figure 1. Transcriptomic and Proteomic Changes Elicited by YBX3 Knock Down

(A) Schematic of approach to identify genes affected by knock down (KD) of YBX3 in HeLa cells. Cells transfected with either non-targeting or YBX3 siRNAs were subjected to a 2-h pulse with metabolic labels (AHA, azidohomoalanine indicated with the red star; SILAC, stable isotope labeling amino acids in cell culture; dark blue represents [13C6,15N2] L-Lys/[13C6,15N4] L-Arg, i.e., heavy, and light blue represents [4,4,5,5-D4] L-Lys/[13C6] L-Arg, i.e., medium) 2 days after siRNA transfection. AHA-containing proteins are coupled to alkyne-agarose by a click chemistry reaction, and *de novo* protein synthesis was measured by quantitative mass spectrometry, while RNA-seq of total RNA measured changes in transcript levels.

(legend continued on next page)

datasets uncover a previously unknown function for YBX3 in regulating amino acid homeostasis. We show that YBX3 stabilizes the mRNAs encoding the amino acid transporters *SLC7A5* and *SLC3A2* by binding to their 3′ UTRs. Importantly, YBX3 depletion reduces the intracellular concentrations of amino acids transported by SLC7A5/SLC3A2, which can be partially recovered by expression of an exogenous SLC7A5 not regulated by YBX3. Thus, our data establish a direct molecular function of YBX3 and reveal its unanticipated role in amino acid transport.

RESULTS

Identification of Genes Affected by YBX3 Depletion

To identify genes whose expression is controlled by YBX3, we used omics techniques to identify changes occurring at both the transcriptomic and translational levels in HeLa cells depleted of YBX3 by small interfering RNA (siRNA). Efficient knockdown (KD) (<10% protein) was achieved after YBX3 depletion for 48 h (Figure S1A). We first examined changes in transcript levels comparing YBX3 KD versus control KD cells by RNA sequencing (RNA-seq) (Figure 1A). Out of the 28,066 detected transcripts, 560 RNAs changed in expression upon YBX3 KD (absolute fold change [FC] > 1.5 with <1% false discovery rate [FDR]; Figure 1B). Of these, 216 transcripts had increased expression, while 344 were decreased in their expression (Figure 1B, red dots indicate significant transcript defined by absolute FC > 1.5 with <1% FDR and orange dots are candidates transcripts defined by absolute FC > 1.5 with <5% FDR). Most of the observed changes are among low-abundant mRNAs with a few distinct exceptions (e.g., *SLC3A2* and *SLC7A5*) (Figure S1D) and did not widely vary between samples (Figure S1C). In parallel samples, we measured protein synthesis by pulse labeling with stable-isotope-labeled amino acids (SILAC) and the methionine analog azidohomoalanine (AHA) to identify and enrich for newly synthesized proteins (Eichelbaum and Krijgsveld, 2014). This method measures the synthesis rate of proteins during the pulse, thus allowing for the analysis of translation when combined with transcriptomic data. In total, we identified 1,869 newly synthesized proteins, 34 of which displayed altered synthesis upon YBX3 depletion in both replicates (absolute FC > 1.5 with 5% FDR; Figure 1C). Specifically, 19 proteins displayed reduced synthesis upon loss of YBX3, whereas 15 proteins showed increased synthesis (Figure 1C, red dots indicate significant proteins defined by absolute FC > 1.5 with <5% FDR and orange dots are candidates proteins defined by absolute FC > 1.5 with <10% FDR). As expected, YBX3 was consistently and significantly reduced at the transcript (Figure 1B), protein synthesis,

and steady-state level (Figures 1C and S1B, respectively) in all replicates.

To determine if the changes in protein translation correlate with altered transcript levels, we integrated the two datasets (Figure 1D; Table S1). The majority of proteins (13 out of 15) with increased expression display little to no corresponding alteration in mRNA levels (Figures 1D and 1E), whereas all proteins with reduced expression show concomitant decreases in mRNA amounts and translation rates with the exception of DNAJA3, which was not identified in the RNA-seq dataset (Figures 1D and 1E). These results suggest that YBX3 regulates gene expression at multiple levels, namely as a translational repressor (i.e., proteins with increased synthesis but no change in mRNA in response to YBX3 deficiency) and a positive regulator of mRNA abundance (i.e., proteins with decreased synthesis and mRNA levels in cells depleted of YBX3). However, the data do not distinguish if the regulation of mRNA abundance occurs at the transcriptional or post-transcriptional level.

YBX3 Binds the 3′ UTR and CDS of Specific mRNAs

The observed changes in gene expression could be a direct or indirect consequence of regulation by YBX3. To uncover direct targets of YBX3, we determined the subset of transcripts that are both bound by YBX3 and show YBX3-dependent gene regulation. To identify YBX3-bound RNAs, we performed eCLIP of YBX3-RNA complexes from HeLa cells (Figure S2A) (Van Nostrand et al., 2016). In total, we generated three YBX3 immunoprecipitation (IP) replicates (with an average of 24.4 million uniquely mapped reads per sample) and three replicates of SMI (size-matched input) controls (with an average of 1.2 million uniquely mapped reads per sample) (Figures S2B and S2C). By normalizing the immunoprecipitated RNA for the RNA abundance obtained from the SMI samples, we found that YBX3 binds a set of specific RNAs broadly without a discernible binding-motif (8,727 binding regions within 4,018 RNAs; Figure 2A). YBX3 binding was enriched within the 3′ UTRs and coding sequences (CDS) of mRNAs, whereas other mRNA regions or types of RNAs, including abundant RNAs (e.g., rRNAs), were depleted from the YBX3 eCLIP samples (Figure 2B). Furthermore, metagene analysis of the transcriptomic region revealed an enrichment of crosslinking within the last third of the transcript (Figure 2C). These data indicate that YBX3 primarily binds mRNAs toward their 3′ ends.

When combining both the significant and candidate categories of differentially expressed genes from the RNA-seq (absolute FC > 1.5 with <5% FDR) and pulse stable isotope labeling by amino acids in cell culture (pSILAC)/AHA datasets

(B) Volcano plot of altered transcripts in cells from (A). RNAs were classified in 3 categories: significant (absolute FC > 1.5 with <1% FDR, red dots), candidate (absolute FC > 1.5 with <5% FDR, orange dots), or not significant (gray dots). From a total of 28,066 RNAs, we identified 560 significantly altered and 110 candidate transcripts; labels are significant transcripts with absolute FC of >3 and SLC7A5 with absolute FC of ~2.6.

(C) Scatterplot of altered *de novo* protein synthesis in YBX3 versus control KD cells with altered proteins classified as significant (absolute FC > 1.5 with <5%FDR, red dots), candidate (absolute FC > 1.5 with <10% FDR, orange dots), or not significant (gray dots). In total, 1,869 proteins were identified with 34 significant and 49 candidate proteins; labels are significant proteins with absolute FC > 2.

(D) Scatterplot integrating proteomic (y axis) and RNA-seq (x axis) datasets. Classification of categories same as in (B) and (C) with red dots found in both datasets and orange and blue dots found in either dataset; labels are significant genes from (C) with an absolute FC of >2.

(E) Bar graph illustrating protein (brown) and transcript (blue) levels for all significant genes from (C). Data provided in Table S1.
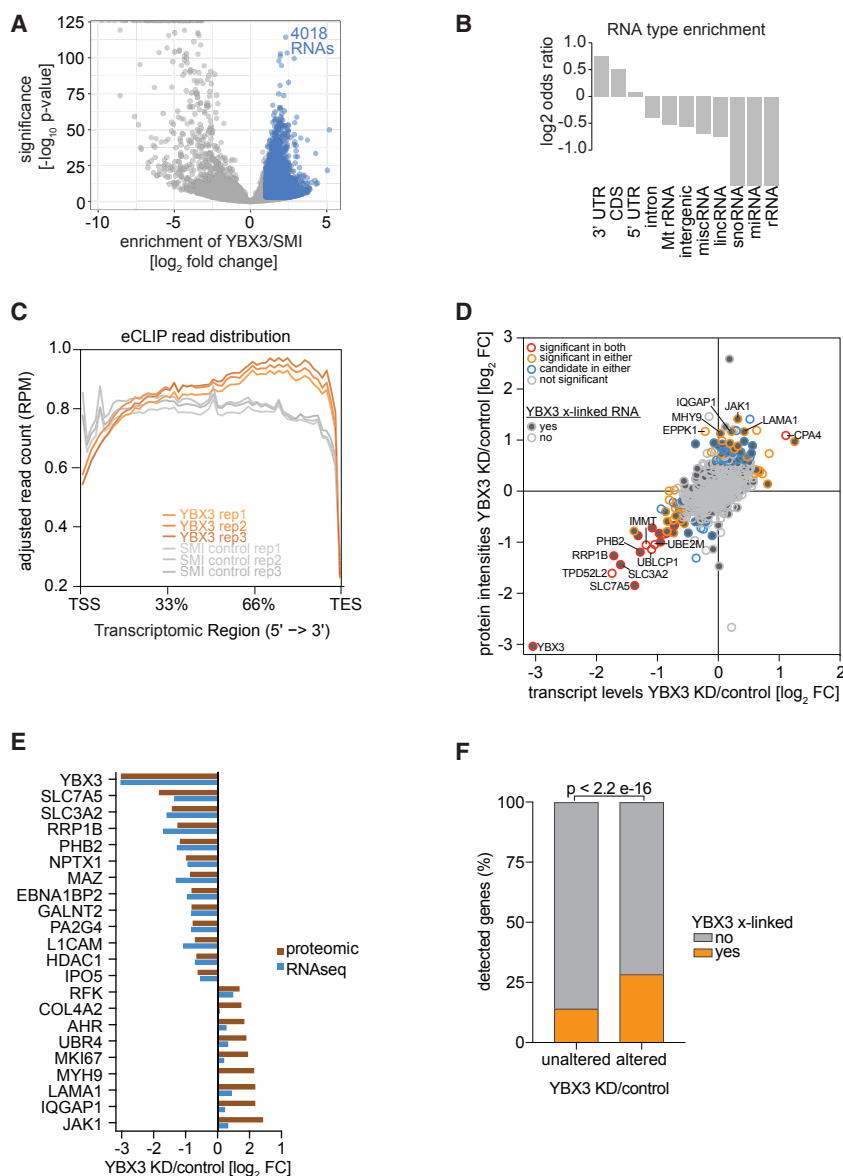
Figure 2. YBX3 Binds mRNA 3′ Ends and Is Enriched in Binding mRNAs Affected by YBX3 Depletion

(A) Visualization of eCLIP enrichment for YBX3 immunoprecipitations versus size-matched inputs (SMIs). Blue dots indicate significantly enriched genomic regions in YBX3 IP (8,727 binding regions within 4,018 RNAs enriched with an absolute FC > 2 with <1% FDR).

(B) RNA type crosslink site enrichment in YBX3 eCLIP compared to SMI control.

(C) Metagene analysis of eCLIP read distribution. Average detectable crosslinks over the transcriptome of RNAs in the YBX3 replicates (orange) versus SMI control (gray). TSS, transcription start site; TES, transcription end site.

(D) Scatterplot integrating the YBX3 eCLIP dataset with integrated proteomics and RNA-seq from Figure 1D.

(E) Bar graph illustrating protein (brown) and transcript (blue) levels for all significant proteins in Figure 1C enriched in YBX3 eCLIP.

(F) Bar graph of YBX3 x-linked RNAs (orange) as a percent of unaltered or altered genes detected in Figures 1B and 1C. In total, 28,202 genes were identified out of which 27,473 were unaltered and 729 were altered by YBX3 KD. Of the unaltered 3,891 (~14.2%) were x-linked by YBX3, while 208 of the altered (~28.5%) were YBX3 x-linked RNAs. A Fisher's exact test for count data was used to determine significance. Data provided in Table S1.

expression at multiple levels, including the control of translational efficiency and mRNA abundance.

YBX3 Enhances the Stability of SLC mRNAs

When looking at the potential direct targets of YBX3, we found two SLCs (SLC7A5 and SLC3A2) (Figure 2D) most substantially altered by YBX3 depletion both at the mRNA and protein level (Figures 1B–1E). Because both proteins are

(absolute FC > 1.5 with <10% FDR), we identify 729 differentially expressed genes. Out of these, only 28.5% (208) are enriched in the YBX3 eCLIP dataset. However, this number increases to nearly 71% (22 bound out of the 31 altered genes) when there is differential protein expression and the transcript is identified in RNA-seq (Figure 2E). These results suggest that altered protein expression frequently results from a direct interaction of YBX3 and the mRNA. We then assessed the percentage of YBX3-bound transcripts comparing those that do or do not respond to YBX3 depletion. Although just over 28.5% of genes with altered expression are enriched in the YBX3 eCLIP data, this number significantly decreases to 14.2% (3891) for genes with unaltered expression in the YBX3 KD (p value$_{Fisher-Exact}$ < 2.2 E-16; Figure 2F; Table S1). Thus, integration of the eCLIP dataset with the proteomic and transcriptomic data indicates that YBX3 directly controls gene

well-known to transport amino acid across the plasma membrane (Baird et al., 2009; Meier et al., 2002; Nicklin et al., 2009), this suggests a possible link between YBX3-directed gene expression and nutrient supply. To dissect how YBX3 regulates the expression of these transporters and perhaps amino acid levels within cells (Figures 1B–1E and 2D), we first assessed the steady-state protein and mRNA levels of these SLCs in YBX3 KD cells. In accordance with the proteomics and RNA-seq data, we found that SLC7A5 and SLC3A2 display reduced steady-state protein and mRNA levels assessed by immunoblotting and quantitative real-time PCR, respectively, whereas the levels of the control mRNAs and proteins were not significantly altered in YBX3 KD cells (Figures 3A and 3B). The levels of the steady-state protein and mRNA reduce to a similar degree, which is in accordance with the results of the integrated proteomic and RNA-seq
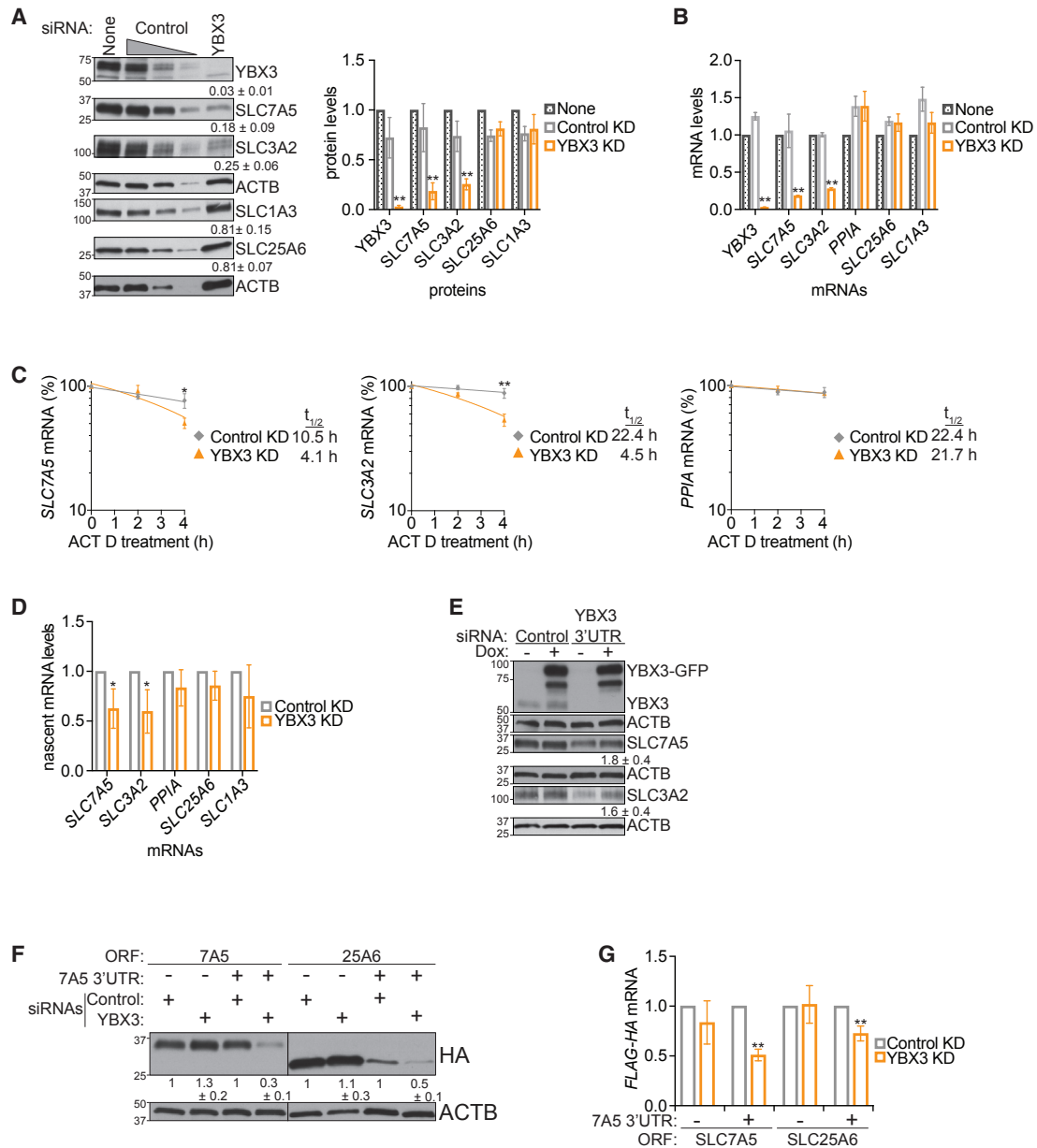
Figure 3. YBX3 Stabilizes Distinct *SLC* mRNAs by Their 3′ UTR

(A) Immunoblot analysis of steady-state protein levels for SLC7A5 and SLC3A2 expression along with negative controls (ACTB, SLC1A3, and SLC25A6). Lysates from cells treated with control siRNAs are loaded at 100%, 50%, and 25%. Protein quantification and molecular mass markers are indicated. PPIA is not represented due to the lack of a suitable antibody.

(B–D) qRT-PCR of relative mRNA levels after YBX3 depletion: (B) steady-state, (C) after actinomycin D (ACT D) treatment, and (D) for nascent mRNA levels after a pulse with 4-thio-uridine (4SU) and enrichment by biotin-streptavidin for indicated transcripts. RNAs extracted at indicated time points after ACT D treatment (C) and 4SU pulse and enrichment method for (D), as described in STAR Methods.

(E) Rescue experiments in doxycycline (Dox)-inducible YBX3-GFP cells. Cells were transfected with siRNAs that only target endogenous YBX3 (3′ UTR specific) or control siRNAs and induced with 0.5 μg/ml Dox for 2 days, lysed, and cell extracts analyzed by immunoblotting with the indicated antibodies. Both SLC7A5 and SLC3A2 have a p value < 0.05 with Student's t test, n ≥ 4.

(F) Immunoblot of control KD or YBX3 KD in Dox-inducible cells expressing SLC7A5- or SLC25A6-FLAG-HA either with or without the SLC7A5 3′ UTR. Protein quantification and molecular mass markers are indicated. Line indicates where the image was cropped to take out superfluous lanes.

(G) qRT-PCR of relative FLAG-HA mRNAs in cells from (F). Protein quantification and molecular mass markers are indicated. All siRNA transfections as in Figure 1A. All qRT-PCR data and immunoblot quantifications are displayed as single points, mean ± SD. **p < 0.01 and *p < 0.05 with Student's t test, n = > 3.

datasets (Figure 1E). Together, these data imply that YBX3 regulates the expression of these SLCs by their mRNA levels.

Transcript levels can be altered by changes in transcription, RNA processing, mRNA stability, or a combination thereof, and YBX3 has been suggested to have roles in all these processes (Balda and Matter, 2000; Coles et al., 1996; Nie et al., 2012; Sourisseau et al., 2006). To address these possibilities, we first evaluated the mRNA half-lives after inhibiting transcription in HeLa cells with actinomycin D. Control mRNAs (PPIA), including other SLC mRNAs (SLC25A6 and SLC1A3) displayed similar half-lives in control and YBX3 KD cells upon blocking transcription (Figure 3C, right panels; Figure S3A). In contrast, YBX3 depletion decreased the mRNA half-lives of the two candidate SLC genes (SLC7A5 and SLC3A2) (Figure 3C, left panels). As YBX3 has also been reported to have roles in transcriptional control (Balda and Matter, 2000; Coles et al., 1996; Sourisseau et al., 2006), we next evaluated the levels of nascent mRNAs after a pulse with 4-thiouridine (4SU), which selectively incorporates into newly transcribed mRNAs, allowing a measurement of transcription of these mRNAs in YBX3 KD (Rädle et al., 2013). This analysis showed a slight, significant reduction in SLC7A5 and SLC3A2 nascent mRNA (~40%) with little to no effect on control mRNAs (Figure 3D). These data suggest that YBX3 affects SLC mRNA abundance at more than one level, including transcriptional and post-transcriptional control.

YBX3 Regulates SLC7A5/SLC3A2 Expression

To follow-up on the finding that YBX3 directly binds the 3′ UTR of these SLC mRNAs, we generated a doxycycline (Dox)-inducible HeLa cell line expressing an siRNA-resistant YBX3-GFP transcript that lacks the YBX3 3′ UTR. In the presence of Dox, an siRNA specifically targeting the 3′ UTR of YBX3 depleted the endogenous protein but not exogenous YBX3-GFP (Figure 3E; Figure S3B). Importantly, YBX3-GFP significantly rescued the reduced protein expression of SLC7A5 and SLC3A2 upon loss of endogenous YBX3 (Figure 3E, lanes 3 and 4). YBX3-GFP also rescued the reduced levels of SLC7A5 and SLC3A2 mRNAs observed upon depletion of endogenous YBX3 (Figure S3C). Together, these results support the notion that YBX3 promotes the expression of SLC7A5 and SLC3A2 proteins by stabilizing their transcripts.

SLC7A5 Regulation by YBX3 Is Mediated by Its 3′ UTR

YBX3 directly binds the 3′ UTR of SLC7A5 (Figure S3D), which is a region that often contains regulatory elements that RBPs bind to stabilize mRNAs (Szostak and Gebauer, 2013). To evaluate the role of the SLC7A5 3′ UTR in YBX3-mediated regulation, we generated Dox-inducible cell lines expressing FLAG-hemagglutinin (HA)-tagged SLC7A5 open reading frames (ORFs) either without (7A5 ORF) or with (7A5 ORF + 7A5 3′ UTR) the SLC7A5 3′ UTR (Figure S3E schematic). We found that the SLC7A5 3′ UTR is required for YBX3-mediated regulation of SLC7A5 protein and transcript levels (Figures 3F, right panels, and 3G). Furthermore, placing the SLC7A5 3′ UTR downstream of the SLC25A6 ORF, an SLC not regulated by YBX3 (Figures 3A and 3B), was sufficient to render the protein and transcript susceptible to regulation by YBX3 (Figures 3F and 3G). The cell lines showed reduced levels of endogenous SLC7A5 and YBX3 upon depletion of

YBX3, as expected (Figures S3E and S3F). Together, these data reveal that the SLC7A5 3′ UTR is required for YBX3-mediated regulation and that YBX3's post-transcriptional control suffices to modulate the expression of SLC7A5 expression.

YBX3 Regulates the Intracellular Levels of Specific Amino Acids by the L1 Transporter

SLC7A5 and SLC3A2 comprise the L1 transporter system, which transports large neutral and aromatic amino acids (LNAA: leucine, isoleucine, phenylalanine, methionine, tyrosine, histidine, tryptophan, and valine). Of note, this includes seven of the nine essential amino acids in human cells (Wu, 2009; Zhang et al., 2017). LNAA import is paired with export of other amino acids at a 1:1 stoichiometry (Figure 4A) (Baird et al., 2009; Meier et al., 2002; Nicklin et al., 2009). To determine if YBX3-mediated regulation of SLC7A5/SLC3A2 affects cellular amino acid levels, we performed targeted metabolomics. Compared to extracts from control cells, YBX3 KD cell extracts displayed significantly reduced levels of all tested SLC7A5/SLC3A2 substrate amino acids (Figure 4B, top). In contrast, amino acids that are not transported by the L1 complex were generally not affected or show minor reductions in their levels (e.g., threonine and lysine) (Figure 4B, bottom). These mild decreases are likely due to reduced SLC3A2 expression, which complexes with other transporters (e.g., SLC7A8 or SLC7A7) to import overlapping but distinct sets of amino acids (Fotiadis et al., 2013; Kandasamy et al., 2018; Verrey et al., 2004). Immunoblotting confirmed that both the transporters and YBX3 were depleted, whereas control proteins were unaffected (Figure S4A). These results suggest that YBX3 is required to maintain intracellular steady-state LNAA levels by regulating SLC7A5/SLC3A2 expression.

The 3′ UTR of SLC7A5 Is Required for YBX3-Mediated Regulation of LNAA Levels

SLC3A2 is a regulatory glycoprotein that is needed to stabilize and transport SLC7A5 to the plasma membrane, whereas SLC7A5 is the subunit necessary for the transport of LNAAs. SLC3A2 interacts with several members of the SLC7 family, and expression of SLC7A5 most closely matches the function of the L1 transporter system (Fotiadis et al., 2013; Kanai et al., 1998; Mastroberardino et al., 1998; Verrey et al., 2004). As SLC7A5 harbors the permease activity for LNAAs, and SLC7A5 regulation by YBX3 is mediated by the 3′ UTR (Figures 3G and 3H), we tested whether ectopic expression of SLC7A5 from a transgene lacking the endogenous 3′ UTR (7A5 ORF) would at least partially restore L1 transporter activity and abrogate the reduction in LNAA levels observed in YBX3 KD cells (Figure 4B). Exogenous 7A5 ORF and 7A5 ORF + 7A5 3′ UTR were expressed at 5-fold and 10-fold lower levels, respectively, than endogenous SLC7A5, and only 7A5 ORF was not reduced upon depletion of YBX3 (Figure 4C, anti-SLC7A5 and anti-HA). Importantly, although LNAA levels were significantly reduced in YBX3 KD cells expressing 7A5 ORF + 7A5 3′ UTR (Figure 4D, bottom), they were substantially restored in YBX3 KD cells expressing the SLC7A5 ORF without the 3′ UTR (Figure 4D, top). These responses are specific because amino acids not transported by the L1 complex were largely unaffected (Figure 4D; Figure S4B).
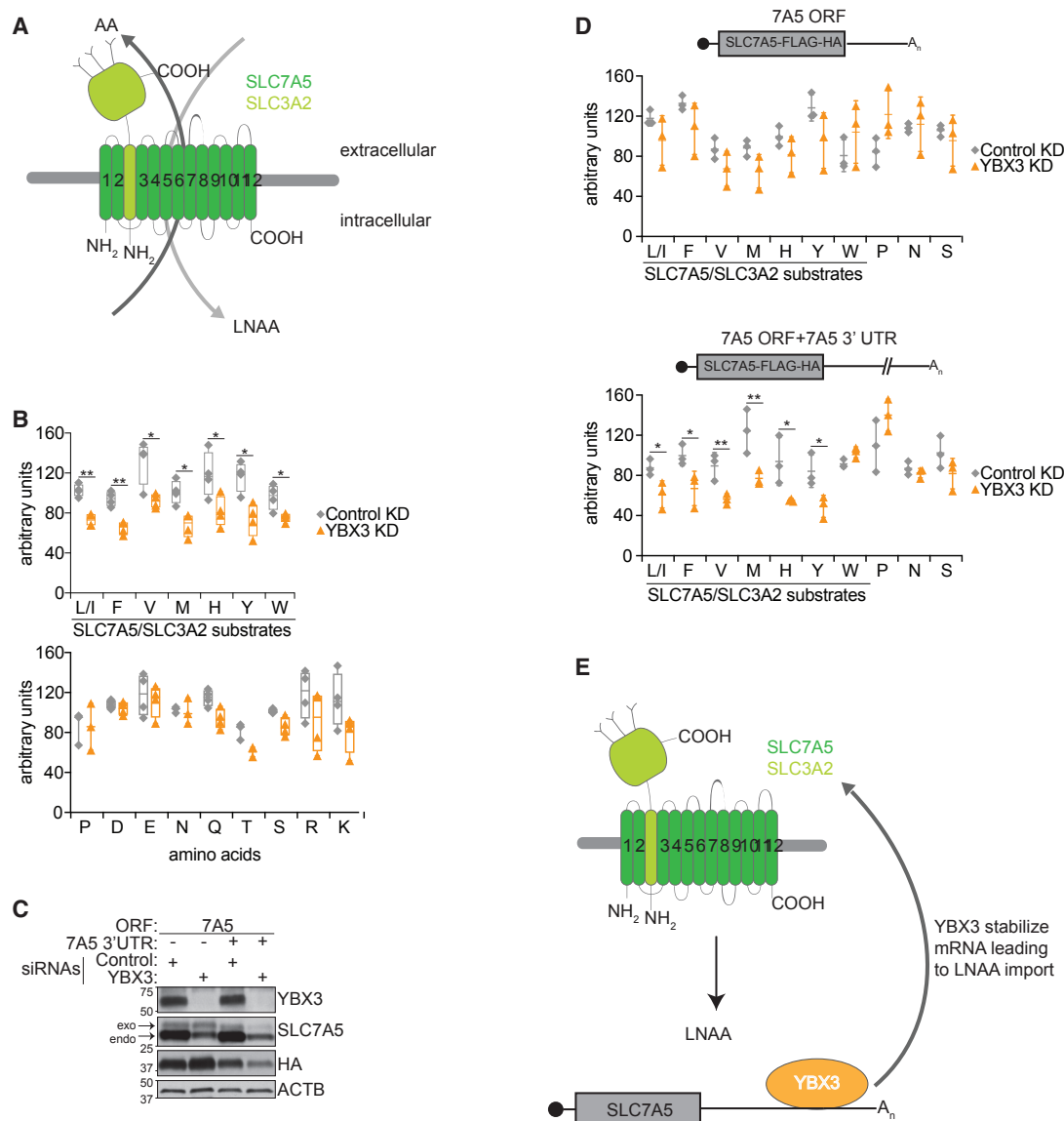
Figure 4. The *SLC7A5* 3′ UTR Sensitizes LNAA Steady-State Levels to YBX3 Regulation

(A) Schematic of SLC7A5/SLC3A2 amino acid transport. Light green, SLC3A2; dark green, SLC7A5; LNAA, large neutral amino acids.

(B) Intracellular amino acid levels after transfection with control or YBX3 siRNAs. Boxplot indicates standard deviation and the line marks median value for the replicates with ** ≤ 1% FDR and * ≤ 5% FDR. SLC7A5/SLCA2 amino acid substrates underlined.

(C) Immunoblot analysis of siRNA transfection in Dox-inducible cell expressing SLC7A5 with or without the 3′ UTR. Marker molecular weight indicated.

(D) Intracellular amino acids in the SLC7A5-inducible cell line without the 3′ UTR (top) or with the 3′ UTR (bottom). Dot plot indicates standard deviation and the line marks average value for the replicates with ** ≤ 1% FDR and * ≤ 5% FDR using the Benjamini, Krieger, and Yekutieli method.

(E) Model of YBX3 regulation of amino acid transport by primarily post-transcriptional control of SLC7A5 and SLC3A2 mRNA stability.

Thus, YBX3 specifically regulates LNAA levels by regulating *SLC7A5* mRNA stability by its 3′ UTR.

DISCUSSION

In contrast to unicellular organisms and plants, mammalian cells synthesize only eleven of the twenty amino acids encoded by the genetic code, whereas the remaining essential amino acids require fine-tuned, active transport (Wu, 2009; Zhang et al.,

2017). SLC protein complexes, such as the L1 system, form the core of specialized transporters that facilitate the exchange of amino acids across membranes (Fotiadis et al., 2013; Hediger et al., 2013; Verrey et al., 2004). As SLCs control the pool of LNAA, their expression is coordinated by a number of processes ranging from transcription to protein stability (Arif et al., 2017; Bröer and Bröer, 2017; Fotiadis et al., 2013; Hediger et al., 2013; Lin et al., 2015; Verrey et al., 2004). Our study reveals an important physiological role of YBX3 as an RBP that regulates

LNAA transport through combined transcriptional and post-transcriptional control of the SLCs SLC7A5 and SLC3A2. Depletion of YBX3 reduces the transcript levels of *SLC7A5* and *SLC3A2* (Figure 3A) by decreasing transcription (Figure 3D) and destabilizing the mRNAs (Figure 3C), which reduces SLC7A5 and SLC3A2 protein levels (Figure 3A) and ultimately attenuates steady-state levels of LNAAs (Figure 4B). YBX3 directly binds the 3′ UTR of *SLC3A2* and *SLC7A5* (Figure 2; Table S1), and this region is required for YBX3 to stabilize the *SLC7A5* mRNA needed for SLC7A5 protein expression (Figures 3G and 3H). LNAA transport is largely uncoupled from YBX3-mediated regulation in cells expressing exogenous *SLC7A5* mRNA lacking the 3′ UTR, demonstrating that the post-transcriptional control is sufficient to affect LNAA steady-state levels (Figure 4D).

Our results highlight YBX3 as a nucleic-acid-binding protein that directly regulates gene expression by using different mechanisms. Specifically, YBX3 acts as a translational repressor (e.g., MYH9 and SPTBN1) and positive regulator of mRNA stability (SLC7A5 and SLC3A2) (Figures 1D, 1E, and 2D). Although this study focuses on the post-transcriptional control of the amino acid transporters, our datasets reflect how YBX3 regulates RNA expression by different mechanisms. RBPs typically regulate their mRNA targets by binding to specific sequences and/or structures within their UTR, which, in turn, assemble complexes dictating an mRNA's fate (Singh et al., 2015). Biocomputational investigations for specific features within the YBX3 eCLIP RNAs did not yield any obvious sequence or structural motifs. However, because the YBX proteins display functional redundancy (Lu et al., 2006; Snyder et al., 2015), our functional analyses in YBX3 depletion cells only yield those YBX3 targets that are not redundantly controlled by the other YBX proteins. Further research needs to be done in examining the features needed for translational repression versus mRNA stability and the overlapping functions among the YBX protein members to characterize the full range of regulation by this protein family.

RNA binding of RBPs can be altered by metabolic cues. Such post-translational regulation was observed nearly three decades ago for IRP1 (e.g., iron regulatory protein 1), where low levels of cellular iron convert cytosolic aconitase into the RBP. IRP1 binds and regulates mRNAs encoding iron transporters for cells (e.g., ferroportin and transferrin receptor 1) to counterbalance the lack of iron (Hentze et al., 1989; Muckenthaler et al., 2017). The expression of specific SLC transporters is sensitive to amino acid levels within cells. For example, SLC38A2, SLC1A5, and SLC7A1 are bound by the RBPs hnRNPL and PTB or HuR respectively, to increase cap-independent translation in response to amino acid starvation (Gaccioli et al., 2006; Majumder et al., 2009; Yaman et al., 2003; Yaman et al., 2002). As YBX3 regulates amino acid levels by its control of SLC7A5/SLC3A2, an interesting possibility is that amino acid levels may instruct this regulation. In fact, YBX3 translation is acutely sensitive to the mechanistic target of rapamycin complex 1 (mTORC1), which is a well-characterized cellular amino acid sensor (Bröer and Bröer, 2017; Thoreen et al., 2012). YBX3 translation is reduced upon inhibition of mTORC1 by the specific inhibitor Torin-1 (Thoreen et al., 2012), suggesting that YBX3 expression is potentially regulated

by cellular amino acids by mTORC1 activity, which, in turn, regulates SLC transporter expression and the import of essential amino acids. There are numerous examples of physiological and pathological conditions that require increases in SLC expression, including T cell activation, cell growth, and development, as well as cancer and inflammatory diseases (Fotiadis et al., 2013; Ren et al., 2017; Scalise et al., 2018). For example, SLC7A5 and SLC3A2 expression rapidly increase in human skeletal muscle after essential amino acid ingestion, which was suggested to be an adaptive response needed to increase amino acid uptake after eating (Drummond et al., 2010). Intriguingly, YBX3 is the only YBX protein detected in human skeletal muscle (The UniProt Consortium, 2017; Uhlén et al., 2015). Therefore, it may be particularly informative to further study YBX3-mediated regulation of amino acid transport in skeletal muscle, which provides a system not complicated by functional redundancy from other YBX proteins and physiological context. Lastly, as SLC7A5 is highly expressed in many human cancers, this work potentially opens up avenues for using YBX3 regulation in therapeutic strategies (Fotiadis et al., 2013; Scalise et al., 2018).

STAR★METHODS

Detailed methods are provided in the online version of this paper and include the following:

- KEY RESOURCES TABLE
- CONTACT FOR REAGENT AND RESOURCE SHARING
- EXPERIMENTAL MODEL AND SUBJECT DETAILS
- METHOD DETAILS
  ○ siRNA Transfections
  ○ Pulse (p)SILAC/AHA Cell Treatment
  ○ Sample Preparation for Mass Spectrometry (MS)
  ○ LC-MS/MS
  ○ Peptide Identification and Quantification
  ○ Data Analysis
  ○ Sample Preparation for RNaseq
  ○ RNaseq Data Analysis
  ○ eCLIP analysis
  ○ eCLIP Data Analysis
  ○ Western Blots
  ○ RNA Extraction and RT-qPCR Analysis
  ○ Actinomycin D RNA Stability Assay
  ○ 4-Thiouridine Pulse for Newly Transcribed RNA
  ○ Plasmids Generated
  ○ Sample Preparation for Targeted Metabolomics of Intracellular Amino Acids
  ○ LC-MS/MS method for Amino Acid (AA) analysis
  ○ Quality Control and Analysis Sequence
  ○ Data Analysis
- QUANTIFICATION AND STATISTICAL ANALYSIS
- DATA AND SOFTWARE AVAILABILITY

SUPPLEMENTAL INFORMATION

Supplemental Information can be found online at https://doi.org/10.1016/j.celrep.2019.05.039.

AUTHOR CONTRIBUTIONS

A.C. designed, performed, and analyzed all experiments with feedback from M.W.H. I.H. contributed to mRNA stability, nascent transcript, RNA-seq, metabolomic, and SLC-reporter experiments and provided advice throughout. T.S. and P.M. analyzed YBX3 eCLIP data, and T.S. analyzed RNA-seq data. T.S. and A.C. performed data integration of transcriptomics, proteomics, and eCLIP. G.K. performed the quantitative mass spectrometry data, and T.S. and G.K. performed data analysis of the quantitative mass spectrometry. A.-M.A. provided technical support for experimental setup. A.C. and M.W.H. wrote the manuscript with input from all authors.

DECLARATION OF INTERESTS

The authors declare no competing interests.

REFERENCES

Arif, W., Datar, G., and Kalsotra, A. (2017). Intersections of post-transcriptional gene regulatory mechanisms with intermediary metabolism. Biochim. Biophys. Acta. Gene Regul. Mech. *1860*, 349–362.

Baird, F.E., Bett, K.J., MacLean, C., Tee, A.R., Hundal, H.S., and Taylor, P.M. (2009). Tertiary active transport of amino acids reconstituted by coexpression of System A and L transporters in Xenopus oocytes. Am. J. Physiol. Endocrinol. Metab. *297*, E822–E829.

Balda, M.S., and Matter, K. (2000). The tight junction protein ZO-1 and an interacting transcription factor regulate ErbB-2 expression. EMBO J. *19*, 2024–2033.

Balda, M.S., Garrett, M.D., and Matter, K. (2003). The ZO-1-associated Y-box factor ZONAB regulates epithelial cell proliferation and cell density. J. Cell Biol. *160*, 423–432.

Bröer, S., and Bröer, A. (2017). Amino acid homeostasis and signalling in mammalian cells and organisms. Biochem. J. *474*, 1935–1963.

Chen, C.Y., Ezzeddine, N., and Shyu, A.B. (2008). Messenger RNA half-life measurements in mammalian cells. Methods Enzymol. *448*, 335–357.

Coles, L.S., Diamond, P., Occhiodoro, F., Vadas, M.A., and Shannon, M.F. (1996). Cold shock domain proteins repress transcription from the GM-CSF promoter. Nucleic Acids Res. *24*, 2311–2317.

Coles, L.S., Bartley, M.A., Bert, A., Hunter, J., Polyak, S., Diamond, P., Vadas, M.A., and Goodall, G.J. (2004). A multi-protein complex containing cold shock domain (Y-box) and polypyrimidine tract binding proteins forms on the

vascular endothelial growth factor mRNA. Potential role in mRNA stabilization. Eur. J. Biochem. *271*, 648–660.

Cox, J., and Mann, M. (2008). MaxQuant enables high peptide identification rates, individualized p.p.b.-range mass accuracies and proteome-wide protein quantification. Nat. Biotechnol. *26*, 1367–1372.

Davies, H.G., Giorgini, F., Fajardo, M.A., and Braun, R.E. (2000). A sequence-specific RNA binding complex expressed in murine germ cells contains MSY2 and MSY4. Dev. Biol. *221*, 87–100.

Dobin, A., Davis, C.A., Schlesinger, F., Drenkow, J., Zaleski, C., Jha, S., Batut, P., Chaisson, M., and Gingeras, T.R. (2013). STAR: ultrafast universal RNA-seq aligner. Bioinformatics *29*, 15–21.

Drummond, M.J., Glynn, E.L., Fry, C.S., Timmerman, K.L., Volpi, E., and Rasmussen, B.B. (2010). An increase in essential amino acid availability upregulates amino acid transporter expression in human skeletal muscle. Am. J. Physiol. Endocrinol. Metab. *298*, E1011–E1018.

Eichelbaum, K., and Krijgsveld, J. (2014). Rapid temporal dynamics of transcription, protein synthesis, and secretion during macrophage activation. Mol. Cell. Proteomics *13*, 792–810.

Fotiadis, D., Kanai, Y., and Palacín, M. (2013). The SLC3 and SLC7 families of amino acid transporters. Mol. Aspects Med. *34*, 139–158.

Gaccioli, F., Huang, C.C., Wang, C., Bevilacqua, E., Franchi-Gazzola, R., Gazzola, G.C., Bussolati, O., Snider, M.D., and Hatzoglou, M. (2006). Amino acid starvation induces the SNAT2 neutral amino acid transporter by a mechanism that involves eukaryotic initiation factor 2alpha phosphorylation and cap-independent translation. J. Biol. Chem. *281*, 17929–17940.

Giorgini, F., Davies, H.G., and Braun, R.E. (2001). MSY2 and MSY4 bind a conserved sequence in the 3′ untranslated region of protamine 1 mRNA in vitro and in vivo. Mol. Cell. Biol. *21*, 7010–7019.

Giorgini, F., Davies, H.G., and Braun, R.E. (2002). Translational repression by MSY4 inhibits spermatid differentiation in mice. Development *129*, 3669–3679.

Hediger, M.A., Clémençon, B., Burrier, R.E., and Bruford, E.A. (2013). The ABCs of membrane transporters in health and disease (SLC series): introduction. Mol. Aspects Med. *34*, 95–107.

Hentze, M.W., Rouault, T.A., Harford, J.B., and Klausner, R.D. (1989). Oxidation-reduction and the molecular mechanism of a regulatory RNA-protein interaction. Science *244*, 357–359.

Ignatiadis, N., Klaus, B., Zaugg, J.B., and Huber, W. (2016). Data-driven hypothesis weighting increases detection power in genome-scale multiple testing. Nat. Methods *13*, 577–580.

Kanai, Y., Segawa, H., Miyamoto, Ki., Uchino, H., Takeda, E., and Endou, H. (1998). Expression cloning and characterization of a transporter for large neutral amino acids activated by the heavy chain of 4F2 antigen (CD98). J. Biol. Chem. *273*, 23629–23632.

Kandasamy, P., Gyimesi, G., Kanai, Y., and Hediger, M.A. (2018). Amino acid transporters revisited: New views in health and disease. Trends Biochem. Sci. *43*, 752–789.

Kleene, K.C. (2018). Y-box proteins combine versatile cold shock domains and arginine-rich motifs (ARMs) for pleiotropic functions in RNA biology. Biochem. J. *475*, 2769–2784.

Kramer, G., Sprenger, R.R., Back, J., Dekker, H.L., Nessen, M.A., van Maarseveen, J.H., de Koning, L.J., Hellingwerf, K.J., de Jong, L., and de Koster, C.G. (2009). Identification and quantitation of newly synthesized proteins in Escherichia coli by enrichment of azidohomoalanine-labeled peptides with diagonal chromatography. Mol Cell Proteomics *8*, 1599–1611.

Kudo, S., Mattei, M.G., and Fukuda, M. (1995). Characterization of the gene for dbpA, a family member of the nucleic-acid-binding proteins containing a cold-shock domain. Eur. J. Biochem. *231*, 72–82.

Lima, W.R., Parreira, K.S., Devuyst, O., Caplanusi, A., N'kuli, F., Marien, B., Van Der Smissen, P., Alves, P.M., Verroust, P., Christensen, E.I., et al. (2010). ZONAB promotes proliferation and represses differentiation of proximal tubule epithelial cells. J. Am. Soc. Nephrol. *21*, 478–488.

Lin, L., Yee, S.W., Kim, R.B., and Giacomini, K.M. (2015). SLC transporters as therapeutic targets: emerging opportunities. Nat. Rev. Drug Discov. *14*, 543–560.

Lindquist, J.A., and Mertens, P.R. (2018). Cold shock proteins: from cellular mechanisms to pathophysiology and disease. Cell Commun. Signal. *16*, 63.

Love, M.I., Huber, W., and Anders, S. (2014). Moderated estimation of fold change and dispersion for RNA-seq data with DESeq2. Genome Biol. *15*, 550.

Lu, Z.H., Books, J.T., and Ley, T.J. (2006). Cold shock domain family members YB-1 and MSY4 share essential functions during murine embryogenesis. Mol. Cell. Biol. *26*, 8410–8417.

Lyabin, D.N., Eliseeva, I.A., and Ovchinnikov, L.P. (2014). YB-1 protein: functions and regulation. Wiley Interdiscip. Rev. RNA *5*, 95–110.

Majumder, M., Yaman, I., Gaccioli, F., Zeenko, V.V., Wang, C., Caprara, M.G., Venema, R.C., Komar, A.A., Snider, M.D., and Hatzoglou, M. (2009). The hnRNA-binding proteins hnRNP L and PTB are required for efficient translation of the Cat-1 arginine/lysine transporter mRNA during amino acid starvation. Mol. Cell. Biol. *29*, 2899–2912.

Mastroberardino, L., Spindler, B., Pfeiffer, R., Skelly, P.J., Loffing, J., Shoemaker, C.B., and Verrey, F. (1998). Amino-acid transport by heterodimers of 4F2hc/CD98 and members of a permease family. Nature *395*, 288–291.

Matsumoto, K., and Wolffe, A.P. (1998). Gene regulation by Y-box proteins: coupling control of transcription and translation. Trends Cell Biol. *8*, 318–323.

Meier, C., Ristic, Z., Klauser, S., and Verrey, F. (2002). Activation of system L heterodimeric amino acid exchangers by intracellular substrates. EMBO J. *21*, 580–589.

Muckenthaler, M.U., Rivella, S., Hentze, M.W., and Galy, B. (2017). A Red Carpet for Iron Metabolism. Cell *168*, 344–361.

Nicklin, P., Bergman, P., Zhang, B., Triantafellow, E., Wang, H., Nyfeler, B., Yang, H., Hild, M., Kung, C., Wilson, C., et al. (2009). Bidirectional transport of amino acids regulates mTOR and autophagy. Cell *136*, 521–534.

Nie, M., Balda, M.S., and Matter, K. (2012). Stress- and Rho-activated ZO-1-associated nucleic acid binding protein binding to p21 mRNA mediates stabilization, translation, and cell survival. Proc. Natl. Acad. Sci. USA *109*, 10897–10902.

Prabhu, L., Hartley, A.-V., Martin, M., Warsame, F., Sun, E., and Lu, T. (2015). Role of post-translational modification of the Y box binding protein 1 in human cancers. Genes Dis. *2*, 240–246.

Rädle, B., Rutkowski, A.J., Ruzsics, Z., Friedel, C.C., Koszinowski, U.H., and Dölken, L. (2013). Metabolic labeling of newly transcribed RNA for high resolution gene expression profiling of RNA synthesis, processing and decay in cell culture. J. Vis. Exp. *78*, 50195.

Ren, W., Liu, G., Yin, J., Tan, B., Wu, G., Bazer, F.W., Peng, Y., and Yin, Y. (2017). Amino-acid transporters in T-cell activation and differentiation. Cell Death Dis. *8*, e2757.

Ritchie, M.E., Phipson, B., Wu, D., Hu, Y., Law, C.W., Shi, W., and Smyth, G.K. (2015). limma powers differential expression analyses for RNA-sequencing and microarray studies. Nucleic Acids Res. *43*, e47.

Sakura, H., Maekawa, T., Imamoto, F., Yasuda, K., and Ishii, S. (1988). Two human genes isolated by a novel method encode DNA-binding proteins containing a common region of homology. Gene *73*, 499–507.

Scalise, M., Galluccio, M., Console, L., Pochini, L., and Indiveri, C. (2018). The Human SLC7A5 (LAT1): The Intriguing Histidine/Large Neutral Amino Acid Transporter and Its Relevance to Human Health. Front Chem. *6*, 243.

Singh, G., Pratt, G., Yeo, G.W., and Moore, M.J. (2015). The Clothes Make the mRNA: Past and Present Trends in mRNP Fashion. Annu. Rev. Biochem. *84*, 325–354.

Snyder, E., Soundararajan, R., Sharma, M., Dearth, A., Smith, B., and Braun, R.E. (2015). Compound Heterozygosity for Y Box Proteins Causes Sterility Due to Loss of Translational Repression. PLoS Genet. *11*, e1005690.

Sourisseau, T., Georgiadis, A., Tsapara, A., Ali, R.R., Pestell, R., Matter, K., and Balda, M.S. (2006). Regulation of PCNA and cyclin D1 expression and epithelial morphogenesis by the ZO-1-regulated transcription factor ZONAB/DbpA. Mol. Cell. Biol. *26*, 2387–2398.

Szostak, E., and Gebauer, F. (2013). Translational control by 3′-UTR-binding proteins. Brief. Funct. Genomics *12*, 58–65.

The UniProt Consortium (2017). UniProt: the universal protein knowledgebase. Nucleic Acids Res. *45*, D158–D169.

Thoreen, C.C., Chantranupong, L., Keys, H.R., Wang, T., Gray, N.S., and Sabatini, D.M. (2012). A unifying model for mTORC1-mediated regulation of mRNA translation. Nature *485*, 109–113.

Uhlén, M., Fagerberg, L., Hallström, B.M., Lindskog, C., Oksvold, P., Mardinoglu, A., Sivertsson, Å., Kampf, C., Sjöstedt, E., Asplund, A., et al. (2015). Proteomics. Tissue-based map of the human proteome. Science *347*, 1260419.

Van Nostrand, E.L., Pratt, G.A., Shishkin, A.A., Gelboin-Burkhart, C., Fang, M.Y., Sundararaman, B., Blue, S.M., Nguyen, T.B., Surka, C., Elkins, K., et al. (2016). Robust transcriptome-wide discovery of RNA-binding protein binding sites with enhanced CLIP (eCLIP). Nat. Methods *13*, 508–514.

Verrey, F., Closs, E.I., Wagner, C.A., Palacin, M., Endou, H., and Kanai, Y. (2004). CATs and HATs: the SLC7 family of amino acid transporters. Pflugers Arch. *447*, 532–542.

Wolffe, A.P., and Meric, F. (1996). Coupling transcription to translation: a novel site for the regulation of eukaryotic gene expression. Int. J. Biochem. Cell Biol. *28*, 247–257.

Wu, G. (2009). Amino acids: metabolism, functions, and nutrition. Amino Acids *37*, 1–17.

Yaman, I., Fernandez, J., Sarkar, B., Schneider, R.J., Snider, M.D., Nagy, L.E., and Hatzoglou, M. (2002). Nutritional control of mRNA stability is mediated by a conserved AU-rich element that binds the cytoplasmic shuttling protein HuR. J. Biol. Chem. *277*, 41539–41546.

Yaman, I., Fernandez, J., Liu, H., Caprara, M., Komar, A.A., Koromilas, A.E., Zhou, L., Snider, M.D., Scheuner, D., Kaufman, R.J., and Hatzoglou, M. (2003). The zipper model of translational control: a small upstream ORF is the switch that controls structural remodeling of an mRNA leader. Cell *113*, 519–531.

Yuan, M., Breitkopf, S.B., Yang, X., and Asara, J.M. (2012). A positive/negative ion-switching, targeted mass spectrometry-based metabolomics platform for bodily fluids, cells, and fresh and fixed tissue. Nat. Protoc. *7*, 872–881.

Zhang, J., Pavlova, N.N., and Thompson, C.B. (2017). Cancer cell metabolism: the essential role of the nonessential amino acid, glutamine. EMBO J. *36*, 1302–1315.

STAR★METHODS

KEY RESOURCES TABLE

REAGENT or RESOURCE	SOURCE	IDENTIFIER
Antibodies		
Rabbit polyclonal anti-ZONAB	Bethyl Laboratories	Cat#A303-070A; RRID: AB_10893576
Mouse monoclonal anti-YBX3/CSDA clone 4D9	LifeSpan Biosciences	Cat#LS-C105064/70947; RRID: AB_2084778
Rabbit polyclonal anti-LAT1	Cell Signaling	Cat#5347; RRID: AB_10695104
Rabbit polyclonal anti-LAT1	Cosmo Bio Co	Cat#KAL-KE026; RRID: AB_567466
Rabbit polyclonal anti-CD98 (H-300)	Santa Cruz Biotechnology	Cat#sc-9160; RRID: AB_638288
Rabbit mAB anti-EAAT1 (D44E2)	Cell Signaling	Cat#5684; RRID: AB_10695722
Mouse monoclonal anti-HA.11 Epitope Tag (Clone 16B12)	Biolegend	Cat#901502; RRID: AB_2565335
Rabbit polyclonal anti-SLC25A6	Thermo Fisher	Cat#PA5-29199; RRID: AB_2546675
anti-β-ACTIN	Sigma	Cat#A5441; RRID: AB_476744
Chemicals, Peptides, and Recombinant Proteins		
Actinomycin D	Sigma	Cat#A1410
4-thiouridine	Biomol	Cat#T2933
L-AHA	Jena Bioscience	Cat#CLK-AA005
$[^{13}C_6,^{15}N_4]$ L-arginine	Silantes	Cat#201603902
$[^{13}C_6,^{15}N_2]$L-lysine	Silantes	Cat#211603902
$[4,4,5,5-D_4]$L-lysine	Silantes	Cat# 211103913
$[^{13}C_6]$L-arginine	Silantes	Cat#201203902
Critical Commercial Assays		
Maxima RT Kit	Thermo Fisher	Cat#K1671
Lipofectamine RNAiMax	Invitrogen	Cat# 137780755
TrueSeq RNA Sample Preparation Kit V2	Illumina	Cat#RS-122-2001
Alkyne Agarose	Jena Bioscience	Cat#CLK-1032
Zymo Quick RNA MicroPrep	Zymo Research	Cat#R1051
Deposited Data		
YBX3 eCLIP data	This paper	ArrayExpress: E-MTAB-5888
Control versus YBX3 KD RNaseq	This paper	ArrayExpress: E-MTAB-7455
Control versus YBX3 KD pSILAC/AHA	This paper	ProteomeXchange: PXD011592
Raw data for Western Blots	This paper	https://data.mendeley.com/datasets/h3x8hjyxzz/1
Experimental Models: Cell Lines		
Human: HeLa cells	ATCC	Cat#CCL-2; RRID:CVCL_0030
Human: HeLa Flp-In	Elena Dobrikova and Matthias Gromeier Duke University	N/A
Human: HeLa Flp-In YBX3:GFP	This paper	N/A
Human: HeLa Flp-In SLC7A5	This paper	N/A
Human: HeLa Flp-In SLC7A5+SLC7A5 3′ UTR	This paper	N/A
Human: HeLa Flp-In SLC25A6	This paper	N/A
Human: HeLa Flp-In SLC25A6+SLC7A5 3′ UTR	This paper	N/A
Oligonucleotides		
ON-Targetplus YBX3 siRNAa, please refer to Table S2	Dharmacon	Cat#J-015793-05; Cat#J-015793-06; Cat# J-015793-07; Cat# J-015793-08
ON-Targetplus Non-targeting, please refer to Table S2	Dharmacon	Cat# D-001810-01; Cat# D-001810-02; Cat# D-001810-03 Cat# D-001810-04

(Continued on next page)

Continued

REAGENT or RESOURCE	SOURCE	IDENTIFIER
Primers for all quantitative reverse transcription polymerase chain reaction (RT-qPCR) please refer to the Table S2	This paper	N/A
Recombinant DNA		
pCDNA5-FRT-TO-YBX3-GFP	This paper	N/A
pCDNA5-FRT-TO-SLC7A5 and variants	This paper	N/A
pCDNA5-FRT-TO- SLC25A6 and variants	This paper	N/A
Software and Algorithms		
Prism GraphPad	GraphPad Software	Version 7
ImageJ	NIH	https://imagej.net/Welcome
htseq-clip	Hentze and Huber groups at EMBL	https://bitbucket.org/htseq-clip/htseq-clip
YBX3 eCLIP data analysis	This paper	https://git.embl.de/schwarzl/ybx3
STAR RNaseq aligner	Dobin et al., 2013	https://github.com/alexdobin/STAR/releases
DeSeq2	Love et al., 2014	https://bioconductor.org/packages/release/bioc/html/DESeq2.html
MaxQuant	Cox and Mann 2008	Version 1.5.1.2; https://www.maxquant.org/
R software	The R project	Version 3.5.1; https://www.r-project.org/

CONTACT FOR REAGENT AND RESOURCE SHARING

Further information and requests for resources and reagents should be directed to and will be fulfilled by the Lead Contact, Matthias W. Hentze (hentze@embl.de).

EXPERIMENTAL MODEL AND SUBJECT DETAILS

Adherent HeLa cells (human female orgin) (ATCC Cat# CCL-2, RRID:CVCL_0030) were grown at 37°C and 5% CO_2 in DMEM, supplemented with 10% FBS Gold (PAA), 1% Penicillin/Streptomycin (Sigma) and 1% L-glutamine (GIBCO). HeLa FLP-IN T-REx lines were a kind gift from Elena Dobrikova and Matthias Gromeier (at Duke University Medical Center). Cell-line stably expressing doxycycline induced proteins were established following the manufacturer's protocol (Flip In TREx, Invitrogen). Stable cell lines were grown in medium containing blasticidine (5mg/ml) and hygromycin (200mg/ml). Inductions were performed with doxycycline at 500 ng/ml overnight. Cell lines were not authenticated.

METHOD DETAILS

siRNA Transfections
Cells were grown until 70%–80% confluent, trypsinized, counted (Biorad TC20) and 200,000 cells were seeded per well in a 6-well dish for reverse transfection of siRNAs following the manufacturer's recommendations (Lipofectamine RNAiMax, Invitrogen, cat# 137780755). YBX3 and control siRNAs were obtained from Dharmacon (YBX3 pool: SMARTpool ON-Targetplus L-015793-00 or YBX3 3′ UTR targeting: ON-Targetplus L-015793-07; and control pool: ON-Targetplus non-targeting siRNAs 1-4). The siRNA used to target the YBX3s 3′ UTR was YBX3 smartpool J-015793-07. Cells were harvested 48 hours after transfections. All siRNA sequences are in Table S2.

Pulse (p)SILAC/AHA Cell Treatment
All experiments were performed in duplicate with reverse SILAC labels.

To deplete HeLa cells of methionine, arginine and lysine, the cells were washed in warm PBS and incubated for 15 minutes in depletion medium (DMEM non-GMP formulation without methionine, arginine and lysine; GIBCO) with 10% dialyzed FBS (GIBCO), L-glutamine and primocin. Then the cells were incubated in the same medium supplemented with 0.1 mM L-AHA (Jena Bioscience, #CLK-AA05) and either 84 μg/ml [$^{13}C_6,^{15}N_4$] L-arginine and 146 μg/ml [$^{13}C_6,^{15}N_2$]L-lysine or 84 μg/ml [$^{13}C_6$]L-arginine and 146 μg/ml [4,4,5,5-D$_4$]L-lysine (Silantes) for 2 hours (Eichelbaum and Krijgsveld, 2014). The cells were washed, trypsinized, counted and centrifuged (5 minutes at 1,000 g). Samples were resuspended in 1ml PBS then 150ul was removed for isolation of RNA (75ul cell suspension) and protein (75ul cell suspension) analysis. The remaining 850ul of cell suspension was centrifuged (5 minutes at 1,000 g) and used for mass spectrometry analysis.

Sample Preparation for Mass Spectrometry (MS)

From each heavy/medium pulse labeling pair, equal amounts (measured by cell number) were lysed in 900ul of 8M Urea, 0.75M NaCl, 6.2% CHAPS in 300mM HEPES, pH 8, with a probe sonicator, cleared by centrifugation and mixed prior to enrichment. Newly synthesized proteins were enriched on alkyne-agarose beads (Click-iT, Life Technologies, NY). Prior to the click reactions, cell lysates were treated with 15 mM iodoacetamide for 30 minutes at room temperature. [3+2] cycloaddition was performed by incubation of the sample with washed alkyne agarose resin (100 ul slurry) in buffer containing 1 mM Cu(II)SO$_4$, 5 mM Tris((1-hydroxy-propyl-1H-1,2,3-triazol-4-yl)methyl)amine (Jena Bioscience), 10 mM aminoguanidine and 10 mM sodium ascorbate (2 mL total volume) for 2 hours at 40°C, while vigorously shaking at 2000 rpm. Following the cycloaddition, the resin was pelleted, supernatants removed and the resin washed with water prior to a 30 min incubation at 70°C in 10 mM tris(2-carboxyethyl)phosphine and 40 mM 2-chloroacetamide in 0.8% SDS, 200 mM NaCl, 4 mM EDTA, 100 mM Tris pH 8.0 with vigorous shaking. After cooling to room temperature, the resin was transferred to an empty column (Biospin Bio-rad) for extensive washing by gravity flow. Sequentially, the column was washed with 5 mL (~100 column volumes) 100 mM Tris-HCl pH 8.0, 1% SDS, 250 mM NaCl, 5 mM EDTA, 1 mL water, 5 mL 6M Guanidine-HCl, 100 mM Tris-HCl pH 8.0 and5 mL 20% acetonitrile in water (ULCMS grade). Subsequently, the bottom of the column was capped for an on-resin digestion by the addition of 0.5 ug of trypsin (sequencing grade, Promega) in 200 ul 50 mM ammonium bicarbonate pH 8.0 and incubation at 37°C for 16h in an incubation oven. Following the digestion, the resulting peptide mixtures were eluted by positive pressure and one additional elution (200 ul 1% formic acid in water). Finally, the combined eluate was desalted with C18 solid phase cartridges (OASIS, Waters) according to the manufacturer's protocol and resuspended in 0.1% trifluoroacetic acid in water for mass spectrometric analysis.

LC-MS/MS

Samples were injected by an Easy-nLC 1200 nano-UPLC (Thermo Fisher Scientific) onto a trap column (Pepmap, 100 μm x 2cm, C18, 5 μm 100Å pores) and separated on an analytical column (PepMap RSLC 75 μm × 50 cm, nanoViper, C18, 2 μM, 100Å) by applying a multistep gradient (Solvent A: 0.1% formic acid in water, Sovent B: 0.1% formic acid, 80% acetonitrile 29.9% water) from: 3%–50% B over 90 min (2h total run time). Eluting peptides were electro-sprayed by applying 2 kV to a Picotip (20 um inner diameter, 10 um tip) coated emitter (New Objective) into an Orbitrap Fusion Tribrid (Thermo Fisher Scientific) mass spectrometer operated in data-dependent mode of acquisition. The Orbitrap operated in positive mode generated profile spectra at a resolution of 60.000 FWHM, AGC target was 1x10^6, maximum injection time 50 ms. Data-dependent selection (top speed) of the most intense ions (threshold 5x103) for HCD-fragmentation using nitrogen as a collision gas (33% CE) by the Quadrupole (1.6 m/z window), resulting fragments were analyzed by the Linear-Ion-Trap set to rapid scan rate, first mass 120 m/z, AGC Target 1x10^4, maximum injection time of 50 ms. Selected ions were excluded for reselection 40 s with a window of 20 ppm.

Peptide Identification and Quantification

Raw data were processed using MaxQuant (version 1.5.1.2) using standard settings (Cox and Mann, 2008). MS/MS spectra were searched against the human UniProt database. Enzyme specificity was set to trypsin, allowing a maximum of two missed cleavages. Cysteine carbamidomethylation was set as fixed modification. Methionine oxidation, protein N-terminal acetylation, methionine to AHA conversion and AHA conversion to diaminobutyrate and homoserine (Kramer et al., 2009) were used as variable modifications. False discovery rates for peptide and protein identification were set to 1%. Match between runs and re-quantify options were enabled. SILAC labeling multiplicity was set to 3 to accommodate the three possible labeling states a peptide could be in.

Data Analysis

R (3.5.1) was used to pre-process the data, proteins flagged as decoy hits were excluded from any further analysis, and SILAC ratio data and signal intensity data were combined for export. Exported data were subjected to statistical analysis for proteins quantified in both biological replicates using moderated t test with linear models. Multiple hypothesis correction was performed with using Independent Hypothesis Weighting (Ritchie et al., 2015).

Sample Preparation for RNaseq

Total RNA was extracted from 7.5% of cells pulsed with SILAC and AHA for each SILAC label and siRNA treatment using Zymo Quick RNA MicroPrep (#R1051, Zymo Research) kit. RNA integrity was assessed using a 2100Bioanalyzer (Agilent Genomics). Barcoded and stranded RNaseq libraries were prepared from high quality total RNA samples (~200 ng/sample) using the Illumina TruSeq RNA Sample Preparation v2 Kit (Illumina, San Diego, CA, USA) implemented on the liquid handling robot Beckman FXP2. Obtained libraries that passed the QC step were pooled in equimolar amounts; 1.8 pM solution of this pool was loaded on the Illumina sequencer NextSeq 500 and sequenced uni-directionally, generating ~500 million reads of ~85 nucleotides each.

RNaseq Data Analysis

The reads were aligned with STAR to the hg38 genome using Gencode v23 annotation (Dobin et al., 2013). Significantly expressed genes were determined with DESeq2 (Love et al., 2014) comparing YBX3 KD samples against control KD (fold change > 1.5, p-adj < 0.01) with independent hypothesis weighting for false discovery rate control under multiple hypothesis testing (Ignatiadis et al., 2016).

eCLIP analysis

Proliferating HeLa cells were washed, irradiated with UV light at 254 nm (150 mJ/cm2), lysed in lysis buffer (500mM NaCl, 50mM Tris-HCl pH 7.5, 8.5% glycerol, 1mM EDTA pH 8.0, 0.5% Triton X-100, 2mM BME and complete EDTA free protease inhibitor (Roche)) and sonicated (Branson sonifier). Lysates were treated with RNase I (10ul 1:25 dilution/extracts from 8.0 × 106 cells; Ambion) to fragment RNA, after which YBX3 RNA complexes were immunoprecipitated with anti-ZONAB (see antibodies section). A library containing the size-matched input (SMI) was generated for each lysate used for the YBX3 IPs. Standard eCLIP workflow was followed as in Van Nostrand et al. (2016) for preparation of SMI and YBX3 IP libraries. In total, 3 YBX3 and 3 SMI libraries were generated from 3 biological replicates and sequenced on Illumina HiSeq2000 platform (125PE, v4 chemistry).

eCLIP Data Analysis

Raw reads were preprocessed as reported in Van Nostrand et al. (2016), and aligned with STAR to the hg38 genome using Gencode v23 annotation (Dobin et al., 2013). Gene definitions were flattened and exons of coding genes were split into 3′ UTR, 5′ UTR and CDS regions. Introns and non-coding regions were added and crosslink sites were counted using htseq-clip (https://bitbucket.org/htseq-clip/htseq-clip). Enriched regions were determined with DESeq2 (Love et al., 2014) comparing YBX3 IP samples against SMI controls ($\log_2$ fold change > 1, p-adj < 0.01) with independent hypothesis weighting for false discovery rate control under multiple hypothesis testing (Ignatiadis et al., 2016). The crosslink site enrichment in RNA types was calculated using a Fisher's exact test. Log odds ratios of significantly enriched types (p-adj < 0.05) are displayed (Figure 2B).

Western Blots

HeLa cells were washed with PBS and lysed in RIPA buffer (150mM NaCl, 50mM Tris-HCL pH 8.0, 1mM EDTA pH 8.0, 1% NP40, 0.5% sodium deoxy cholate, 0.1% SDS, 1x complete protease inhibitor without EDTA (Roche) and 4 ul/100ul benzonase 1:100(Sigma)). Total protein extracts were run on a 4%–15% TGX gel (Biorad) in 1x Laemmli running buffer, transferred to nitrocellulose membranes using the standard turbo transfer mixed molecular weight program on the trans blot turbo system (Biorad), and analyzed using primary antibodies as follows: anti-ZONAB (Bethyl Laboratories, #A303-070A, RRID:AB_10893576), 1:2000; anti-YBX3/CSDA clone 4D9 (LifeSpan Biosciences, #LS-C105064/70947, RRID:AB_2084778), 1:500; anti-LAT1 (Cell Signaling, #5347, RRID:AB_10695104), 1:2000; anti-LAT1 (Cosmo Bio Co., #KAL-KE026, RRID:AB_567466), 1:1000; anti-CD98 (H-300) (Santa Cruz Biotechnology, #sc-9160, RRID:AB_638288), 1:4000; anti-EAAT1 (D44E2) (Cell Signaling, #5684, RRID:AB_10695722) 1:1000; anti-HA.11 Epitope Tag (Clone 16B12) (Biolegend, #901502, RRID:AB_2565335), 1:5000; anti-SLC25A6 (Thermo Fischer, #PA5-29199, RRID:AB_2546675); anti-β-ACTIN (Sigma, #A5441, RRID:AB_476744), 1:10000. Secondary antibodies used were: goat anti-mouse IgG-HRP (Santa Cruz Biotechnology, #sc-2005, RRID:AB_631736); goat-anti-rabbit IgG-HRP (Santa Cruz Biotechnology, #sc-2004, RRID:AB_631746); goat-anti-rabbit IgG-HRP (Abcam, #97051, RRID:AB_10679369). Amount of secondary antibody was optimized for primary antibody and ranged from 1:5000 to 1:20000.

RNA Extraction and RT-qPCR Analysis

Total RNA was isolated using Zymo Quick RNA MicroPrep (#R1051, Zymo Research) or MiniPrep (#R1055, Zymo Research) kit following the manufacturer's recommendations including the in-column DNAase treatment. 1.0 μg total RNA was used to synthesize cDNA using the Maxima First Strand cDNA Synthesis Kit (#K1672, Thermo Fischer) for quantitative reverse transcription polymerase chain reaction (RT-qPCR). RT-qPCR was performed using the SYBR-Green qPCR Master mix (#4309155, Applied Biosystems) on a StepOne Real-Time PCR System (Applied Biosystems). Gene expression values were normalized using *GUSB* or *B2M* and are shown as a relative fold change to the value of control siRNA-treated samples. All experiments were performed in biological triplicate and error bars indicate ± standard deviation as assayed by the ΔΔCt method. A Student's t test was used to determine significance in values for control versus YBX3 siRNA samples. All RT-qPCR primers are listed in the table below.

Actinomycin D RNA Stability Assay

HeLa cells were treated with 5 μg/ml actinomycin D (ACT D) (#A1410, Sigma) and RNA was isolated using Zymo Quick RNA MiniPrep at 0 hours (i.e., no treatment), 2 hours, or 4 hours after addition of ACT D. cDNA synthesis and RT-qPCR were performed as in the RNA extraction and RT-qPCR analysis section. RNA decay was measured with normalized RT-qPCR values relative to values at 0 hours for each condition. Half-life values were determined using a semi-logarithmic linear regression analysis to determine the line that best fits the data (Chen et al., 2008).

4-Thiouridine Pulse for Newly Transcribed RNA

HeLa cells were treated with 500uM 4-thiouridine (# T4509 4-thiouridine, Sigma) for 30 minutes at 37°C and total RNA was isolated using Zymo Quick RNA MiniPrep. RNAs transcribed with 4SU were enriched following Rädle et al. (2013). Briefly, 70-85ug of total RNA was labeled with EZ-Link Biotin-HPDP (Pierce), isolated with μMacs Streptavidin columns (# 130-074-101, Miltenyi) and cleaned up with QIAGEN RNeasy MinElute Cleanup Kit (#74204, QIAGEN). 200ng of 4SU labeled RNA was used to produce cDNA using Maxima First Strand cDNA Synthesis Kit followed by standard pRT-PCR (see above).

Plasmids Generated

To generate the expression plasmids for inducible stable cell lines, YBX3 was amplified from HeLa cDNA and cloned into the HindIII and XhoI sites of pCDNA5-Frt-To-Linker-eGFP vector. SLC7A5 or SLC25A6 were amplified from HeLa cDNA, followed by cloning into the HindIII and XhoI sites of pCDNA5-Frt-To-Linker-FLAG-HA. The SLC7A5 3′ UTR was then amplified and cloned into the HindIII and KpnI sites of these vectors. The vectors lacking the SLC7A5 3′ UTR contain a short 3′ UTR from the vector that terminates with a BGH pA sequence. Sanger sequencing verified all constructs. All primers for amplification are listed in Table S2.

Sample Preparation for Targeted Metabolomics of Intracellular Amino Acids

48 hours after control or YBX3 siRNA transfections, cells were harvested for metabolomic analysis following extraction of metabolites in adherent cell lines (Yuan et al., 2012).

LC-MS/MS method for Amino Acid (AA) analysis

Analytical Method

LC-MS/MS analysis was performed on a Vanquish UHPLC system coupled to a Q-Exactive plus HRMS (Thermo Scientific, MA, USA) in both ESI positive and negative mode. The separation of AA was carried out on Xbridge Amide (100X 2.1mm; 2.6uM) at the flow rate of 0.3 ml/min and maintained at 40°C. The mobile phase consisted of solvent A (7.5 mM Ammonium acetate with 0.05% NH4OH) and solvent B (acetonitrile). The UHPLC system was run in gradient mode as described in Table S2. AA were detected with HRMS full scan at the mass resolving power R = 70000 in mass range of 60-900 m/z. The data-dependent tandem (MS/MS) mass scans were obtained along with full scans using higher energy collisional dissociation (HCD) of normalized collision energies of 10, 20 and 30 units which were at the mass resolving power R = 17500. The MS parameters in the Tune software (Thermo Scientific) were set as: spray voltage of 4 kV (for negative mode 3.5 kV), sheath gas 30 and auxiliary gas 5 units, S-Lens 65 eV, capillary temperature 320°C and vaporisation temperature of auxiliary gas was 300°C. Data were acquired in full scan mode and data dependent tandem mass spectra (MS/MS) for all precursors corresponding to targeted AA. For LC gradient used refer to Table S2.

Quality Control and Analysis Sequence

All samples were randomized regarding the LC-MS analysis sequence. The pooled quality control (QC) samples were prepared by mixing equal volumes from each sample and processed in a similar manner. Blank and multiple QC samples were injected at the beginning of the sample analysis sequence in order to stabilize LC-MS system. A QC sample was injected after each 4 samples to track the stability of instrument and analytical method (%CV < 20) throughout the analysis sequence. The chromatograms were evaluated manually and stability of QC samples checked before proceeding for further data analysis.

Data Analysis

The Thermo software Xcalibur Quan was used for data analysis including the generation of extracted ion chromatograms (XIC), peak integration and raw data visualization. The peak areas were exported into spreadsheets for further data analysis, including concentration calculation, quality control (QC) evaluation, blank subtraction, and statistical analyses.

The identity of each AA peak in protonated [M+H] or deprotonated form [M-H] was confirmed by matching its retention time and exact mass (±5 ppm) with respective authentic standards. All data were evaluated for consistency of peak integration, and manual integration was performed whenever necessary. The peak areas for each AA were normalized to cellular protein concentration for each sample, and then arbitrarily scaled so that all values could be plotted together for the plots shown in Figure 4 and Figure S4. GraphPad Prism 7 software was used to determine the False Discovery Rate with the Two-stage linear step-up procedure of Benjamini, Krieger and Yekutieli, with Q = 5%, for changes in amino acid levels between YBX3 and control KD cells.

QUANTIFICATION AND STATISTICAL ANALYSIS

All RT-qPCR data and western blot quantifications are displayed as single points, mean ± SD; Student's t test was used, p < 0.05 was considered statistically significant and n values for biological replicates are indicated in respective Figure legends. Metabolomics data plots individual measurements from the biological replicates, median ± SD; False Discovery Rate with the Two-stage linear step-up procedure of Benjamini, Krieger and Yekutieli, with Q = 5% in GraphPad Prism 7, n values for biological replicate are indicated in the respective Figure legends. GraphPad Prism v7.0 was used to create all plots. Images were quantified with ImageJ (https://imagej.nih.gov/ij/) to determine the relative intensity of protein to the levels of the ACTB loading control on the western blots following the web-based tutorial: https://lukemiller.org/index.php/2010/11/analyzing-gels-and-western-blots-with-image-j/.

DATA AND SOFTWARE AVAILABILITY

The accession number for the pSILAC/AHA proteomics data reported in this paper is "ProteomeXchange: PXD011592." The accession number for the RNaseq and eCLIP datasets reported in this paper is "Array Express: E-MTAB-7455 and E-MTAB-5888," respectively. The analysis of YBX3 eCLIP data can be found at https://git.embl.de/schwarzl/ybx3.